ELSEVIER

Chemical Engineering Science 60 (2005) 5682–5695

Chemical Engineering Science

www.elsevier.com/locate/ces

Support effects in hydrogenation of cinnamaldehyde over carbon nanofiber-supported platinum catalysts: Kinetic modeling

Marjolein L. Toebes[a], T. Alexander Nijhuis[a], Jan Hájek[b], Johannes H. Bitter[a], A. Jos van Dillen[a], Dmitry Yu. Murzin[b], Krijn P. de Jong[a,*]

[a]*Department of Inorganic Chemistry and Catalysis, Debye Institute, Utrecht University, P.O. Box 80 083, 3508 TB Utrecht, Netherlands*
[b]*Laboratory of Industrial Chemistry, Process Chemistry Group, Åbo Akademi University, Turku/Åbo, Finland*

Received 27 September 2004; received in revised form 12 May 2005; accepted 12 May 2005
Available online 29 June 2005

Abstract

Carbon nanofiber-supported platinum catalysts with a narrow and stable platinum particle size distribution (1–2 nm) were prepared, one with a considerable amount of oxygen support surface groups (PtCNF, 2.8 acidic O atoms/nm^2) and one with a much smaller amount (PtCNF973, 0.06 acidic O atoms/nm^2). Their catalytic performance was compared in a series of liquid-phase cinnamaldehyde hydrogenation experiments at 383 K using hydrogen pressures of 2.8–6.8 MPa and a cinnamaldehyde concentration in the range 14–345 mol/m^3. These results showed a different hydrogen dependency of the reaction rate for the two catalysts, demonstrating a change in the adsorption of hydrogen on platinum. Using a single-site model including both Langmuir–Hinshelwood kinetics and mass transfer effects we found that the intrinsic reaction rate increased up to a factor of 120 with the removal of the oxygen-containing surface groups. Also the adsorption constants increased significantly, indicating that adsorption on PtCNF973 is stronger than on PtCNF. These results suggest that hydrogenation is assisted by adsorption of the benzene ring of cinnamaldehyde on the non-polar CNF support surface after removal of the oxygen-containing groups.

Keywords: Catalyst selectivity; Kinetics; Catalyst support; Hydrogenation; Carbon nanofibers; Platinum

1. Introduction

The selective hydrogenation of α,β-unsaturated aldehydes to unsaturated alcohols is a key step especially in the preparation of various fine chemicals and is often used in the literature as a sensitive test reaction (see Kluson and Cerveny, 1995; Ponec, 1997; Coq and Figueras, 1998; Gallezot and Richard, 1998; Hajek et al., 2003). Important factors influencing the activity and selectivity are amongst others, the active metal, the catalyst support properties, the metal particle size and the presence of promoters such as a second metal or alkaline solutions. A very commonly used catalyst system for this type of reactions is platinum supported on graphitic carbon (Coq and Figueras, 1998; Giroir-Fendler et al., 1988; Coq et al., 1993; Kumbhar et al., 1995; van de Moesdijk and Bosma, 1988).

Our study of a series of carbon nanofiber (CNF)-supported platinum catalysts (Toebes et al., 2004a) and earlier work on Ru/CNF catalysts (Toebes et al., 2003) have shown a continuous trend in activity and selectivity in the liquid-phase hydrogenation of cinnamaldehyde with decreasing numbers of oxygen-containing support surface groups. The observed rate of cinnamaldehyde conversion was enhanced by a factor of 22 (Ru) and 25 (Pt) as the number of acidic oxygen-groups per nm^2 decreased from 2.8 to 0.06, mainly due to a strong increase in hydrogenation rate of the C═C bond. Only a slight increase in C═O bond hydrogenation rate was observed, resulting in a large shift in selectivity towards hydrocinnamaldehyde.

* Corresponding author. Tel.: +31 30 2536762; fax: +31 30 2511027
E-mail address: k.p.dejong@chem.uu.nl (K.P. de Jong).

0009-2509/$ - see front matter © 2005 Elsevier Ltd. All rights reserved.
doi:10.1016/j.ces.2005.05.031

A possible explanation for the change in catalytic properties involves an indirect support effect on catalysis via the electronic state of the metal particles. The density of states of the metal particles may shift to a higher binding energy with decreasing electron richness of the support atoms, which influences the catalytic behavior (Ramaker et al., 2001; Koningsberger et al., 2003; Mojet et al., 1999). However, we have shown with XPS and H_2-chemisorption that with the Pt/CNF catalytic system the electronic properties of the platinum particles do not change to a large extent with varying numbers of oxygen-containing groups (Toebes et al., 2004a). Therefore, it is not likely that the changes in catalytic performance with decreasing numbers of oxygen-containing support groups are primarily brought about by an electronic effect.

An alternative explanation for a support effect on the catalytic performance can be found in its involvement in the catalytic action. An extreme example of this is bifunctional catalysis, in which sites on the support are responsible for a part of the catalytic conversion. A case in point is alkane hydro-isomerization with a metal-loaded acidic zeolite. The metal particles exhibit hydrogenation/dehydrogenation activity, whereas the acidic sites of the support exhibit isomerization and cyclization properties. Burch and Flambard were the first describing a more subtle, so-called interfacial metal–support interaction (Burch and Flambard, 1982a,b). They observed that titania-supported nickel particles exhibited a fifty times higher specific activity for the formation of methane from CO/H_2 than silica-supported nickel catalysts due to active sites at the metal–titania interface. Also with gold on titania catalysts the metal–support interface plays an essential role in the CO oxidation by O_2. In this reaction probably oxygen adsorbs on oxygen vacancy sites in the titania surface while CO adsorbs on gold (Haruta et al., 1993; Grunwaldt and Baiker, 1999). For CO_2/CH_4 reforming over zirconia-supported platinum catalysts, Bitter et al. (1997) proposed that CO_2 is activated on the support by formation of carbonate species that react with methane adsorbed on platinum.

We studied to what extent oxygen-containing surface groups on CNF influence the catalytic performance of CNF-supported noble metal catalysts in the hydrogenation of cinnamaldehyde. We found that at increasing treatment temperatures of Pt/CNF, the CNF surface changes gradually from polar to non-polar due to the removal of oxygen-containing surface groups, which might affect the adsorption location or mode of the organic compound and thus the role of the support in the reaction. We have used kinetic modeling to explore the impact of the support on the catalytic action.

Often a first-order rate law has been used to model the cinnamaldehyde hydrogenation experiments, however, this simple rate equation did not describe the cinnamaldehyde kinetics satisfactorily (Galvagno et al., 1991; Poltarzewski et al., 1986; Cerveny et al., 1996; Zhang et al., 1998; Marchi et al., 2003). Tronconi et al. (1990), Neri et al. (1997) and Vergunst et al. (2001) provide a more extensive kinetic model for this complex reaction. Tronconi et al. (1990) and Neri et al. (1997) studied the effect of temperature using Langmuir–Hinshelwood kinetics. They assumed that adsorption of reactants and products is reversible and competitive while hydrogen is activated on a different site and does not compete with the organic compounds. The rate-determining step is considered to be the reaction between atomic hydrogen and the adsorbed organic compound. A two-site model is assumed, one type of site for hydrogenation of the carbonyl bond (C═O) and another type of site for olefinic bond (C═C) hydrogenation. They found that other models (using one type of site only or using competitive hydrogen adsorption) gave less satisfactory results. Vergunst et al. (2001) compared three different kinetic models for the hydrogenation of cinnamaldehyde over Pt/C/monolithic catalysts. A single-site and a two-site model with the surface reactions as rate-controlling steps were unable to fit the experimental data satisfactory. They concluded that a single-site model in which both adsorption, surface reaction and desorption are all rate determining steps gives the best results. However, the effect of hydrogen pressure and initial cinnamaldehyde concentration on the activity and selectivity could not be included in the model successfully.

In the current study two CNF-supported platinum catalysts with small and uniform metal particles (1–2 nm) were investigated, one with a considerable amount of oxygen support surface groups (PtCNF) and one with a much smaller amount (PtCNF973). Their catalytic performance was measured in the liquid-phase hydrogenation of cinnamaldehyde in a semi-batch reactor at 383 K. Kinetic models were used to fit the experimental results obtained with varying concentrations of cinnamaldehyde ($[CALD]_0 = 14–345\ mol/m^3$) and hydrogen pressures ($P_{H_2} = 2.8–6.8$ MPa). Reaction rate constants for the different steps and adsorption constants were derived from the model fits taking into account internal diffusion limitation with the most active catalyst PtCNF973. An explanation for the enhanced activity and shifted selectivity with decreasing oxygen-containing surface groups based on the kinetic modeling results is proposed.

2. Experimental

2.1. Carbon nanofiber growth

For the growth of CNF a 20 wt% Ni/SiO_2 catalyst was prepared by homogeneous deposition precipitation (HDP) as described by Van Dillen et al. (1977) using silica (Degussa, Aerosil 200), nickel nitrate (Acros) and urea (Acros). After filtering the catalyst precursor was dried at 393 K and calcined in static air at 873 K (heating rate 5 K/min) for 2 h. One gram of the Ni-catalyst precursor was placed in a quartz reactor. Prior to the fiber growth the Ni-catalyst precursor was reduced in situ for 2 h in a stream of a mixture of H_2 (80 mL/min) and N_2 (320 mL/min) at 1 bar and 973 K (heating rate 5 K/min). Next, the CNF were grown at 823 K

in a mixture of CO (80 mL/min), H_2 (28 mL/min), and Ar (292 mL/min) for 24 h. A more detailed description of the growth catalyst and the growth of the CNF can be found elsewhere (Toebes et al., 2002). The CNF were refluxed for 1 h in a 1 M KOH solution in order to remove the silica support. For activation by surface oxidation and removal of nickel, the CNF were refluxed in concentrated nitric acid for 2 h and washed thoroughly with demiwater.

2.2. Synthesis carbon nanofiber-supported platinum catalyst

Platinum (intake 5 wt%) was deposited on the fibers according to a homogeneous deposition precipitation method. To an acidified suspension (pH = 3) of 5 g CNF in 250 mL demi-water heated up to 363 K under inert atmosphere, 0.41 g urea (Acros) and 0.52 g $Pt(NH_3)_4(NO_3)_2$ (Aldrich) were added under vigorous stirring. The pH of the slurry was monitored, to follow the process and to indicate its completeness. After 18 h the loaded CNF were filtered and washed thoroughly with demiwater, dried at 353 K in an N_2 flow and reduced in flowing H_2 at 473 K for 1 h (heating rate = 5 K/ min). Next the samples were exposed to air at RT.

A sample of the freshly reduced catalyst (PtCNF) was heat-treated in an N_2 flow for 2 h at 973 K (PtCNF973), to remove (part of) the oxygen-containing groups from the CNF surface.

2.3. Catalytic experiments

The liquid-phase hydrogenation of cinnamaldehyde was studied in a 500 mL stirred semi-batch reactor equipped with a sample port, a reagent injection port, gas inlet and vent.

The catalyst samples (0.2 g), consisting of spherical catalyst particles with an average radius of 60 μm as determined on the basis of SEM images, were re-reduced in *i*-propanol (220 mL) at 383 K and 2.8 MPa H_2 pressure for 30 min in the autoclave (1500 rpm) prior to the introduction of cinnamaldehyde (CALD) (0.40–10.0 g $= 14–345\ mol/m^3$). All reactions were conducted at 383 K using total pressures of 3.0, 5.0 and 7.0 MPa(g). These total pressures result, after correction for the vapor pressure of iso-propanol at 383 K, in hydrogen partial pressures of 2.8, 4.8 and 6.8 MPa. Also experiments with the two primary products, hydrocinnamaldehyde (HALD) and cinnamyl alcohol (CALC), were performed at 383 K and a hydrogen pressure of 4.8 MPa. Samples of the reaction mixture (1–1.5 mL) were withdrawn periodically and analyzed on a gas chromatograph (Hewlett Packard 5890 Series with autosampler) using an HP5 capillary column (30 m × 0.32 mm; 0.25 μm film thickness).

3. Results and discussion

3.1. CNF-supported platinum catalysts

The metal loading of the PtCNF and PtCNF973 catalysts as determined with XRF was found to be 3.6 wt%. In Fig. 1 TEM images of PtCNF and PtCNF973 are shown. The platinum particles of PtCNF are small (1–2 nm) and homogeneously distributed over the support surface. For PtCNF973 the platinum particles are slightly larger, ranging from 1 to 3 nm. From H_2-chemisorption measurements, platinum dispersions of 0.79 and 0.49 were derived corresponding with an average particle size of 1.4 nm for PtCNF and 2.3 nm for PtCNF973. EXAFS data of PtCNF confirm the TEM and H_2-chemisorption results; from the measured coordination number of 5.2, an average particle size of 1.0 nm could be calculated. TEM examination of the spent catalysts demonstrated that during the hydrogenation experiment no significant change in the platinum particle size and distribution had occurred. Although a slight increase in average platinum particle size is observed after heat treatment at 973 K it is highly unlikely that this change in particle size is the main cause of the large increase in activity and the shift in selectivity. First of all, we have demonstrated that a continuous trend was observed in the activity with decreasing

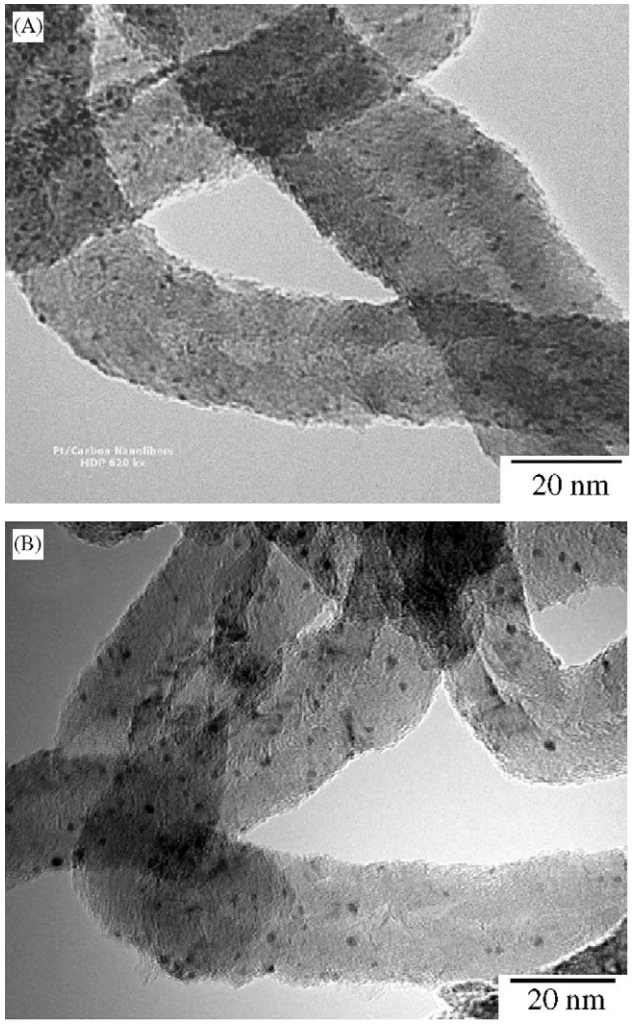

Fig. 1. TEM images of 3.6 wt% CNF-supported platinum catalysts (A) PtCNF and (B) PtCNF973.

numbers of acidic oxygen groups while the average particle sizes of the catalysts treated at 573 and 773 K were similar to the platinum particle size found with PtCNF (Toebes et al., 2004a). Secondly, a particle size effect is unlikely to bring about such huge changes in catalytic performance.

The amount of oxygen present on the CNF support and the Pt/CNF catalysts after the different treatments was assessed using XPS and TGA-MS. With the unloaded supports also acid–base titrations were performed to establish the number of carboxylic sites at the exterior surface of the CNF. PtCNF contains a total number of 6 O atoms/nm^2 while the number of acidic sites corresponds to 2.8 O atoms/nm^2. All techniques showed a lower total number of oxygen (2.4 O atoms/nm^2) and a much lower number of acidic oxygen-containing groups (0.06 O atoms/nm^2) on the catalyst after treatment in nitrogen at 973 K. Our elaborate investigations on the size of the platinum particles of the Pt/CNF catalysts and change in number of (surface) oxygen groups with the pretreatment can be found elsewhere (Toebes et al., 2004a,b).

3.2. Catalytic results

3.2.1. General

Typical concentration-time plots of cinnamaldehyde hydrogenation experiments with both PtCNF and PtCNF973 under standard reaction conditions (103 mol/m^3 CALD, hydrogen pressure 4.8 MPa, $T = 383$ K) are displayed in Fig. 2. Especially for the most active catalyst (PtCNF973) the consecutive reaction is evident, i.e., the primary products HALD and CALC are hydrogenated to hydrocinnamyl alcohol (HALC). From the decrease in the concentration of CALD with time an initial activity was calculated. Under standard reaction conditions for PtCNF the initial activity is 1.9 mmol min^{-1} g_{cat}^{-1} and for PtCNF973 14.9 mmol min^{-1} g_{cat}^{-1}. TOFs of, respectively, 0.23 and 3.3 s^{-1} were found, calculated as mole CALD hydrogenated per mole of platinum surface atom per second. The increased activity of PtCNF973 is mainly caused by a large increase in HALD formation rate as can be seen in Fig. 2. Apparently the rate of hydrogenation of the C=C bond is strongly enhanced when most of the oxygen-containing groups are removed from the CNF surface. The selectivities towards CALC and HALD determined at 60% conversion are 37% and 32% for PtCNF and 8% and 74% for PtCNF973, respectively.

To investigate whether the catalysts became irreversibly deactivated, three consecutive experiments with one batch of catalyst PtCNF were executed. Between the runs the catalyst was washed repeatedly with iso-propanol and dried. The activity of the catalysts in the three runs was comparable, thus proving the absence of irreversible deactivation.

3.2.2. Influence H_2 pressure

Fig. 3 displays the effect of hydrogen pressure on the activity of PtCNF ($[CALD]_0 = 103$ mol/m^3) and PtCNF973

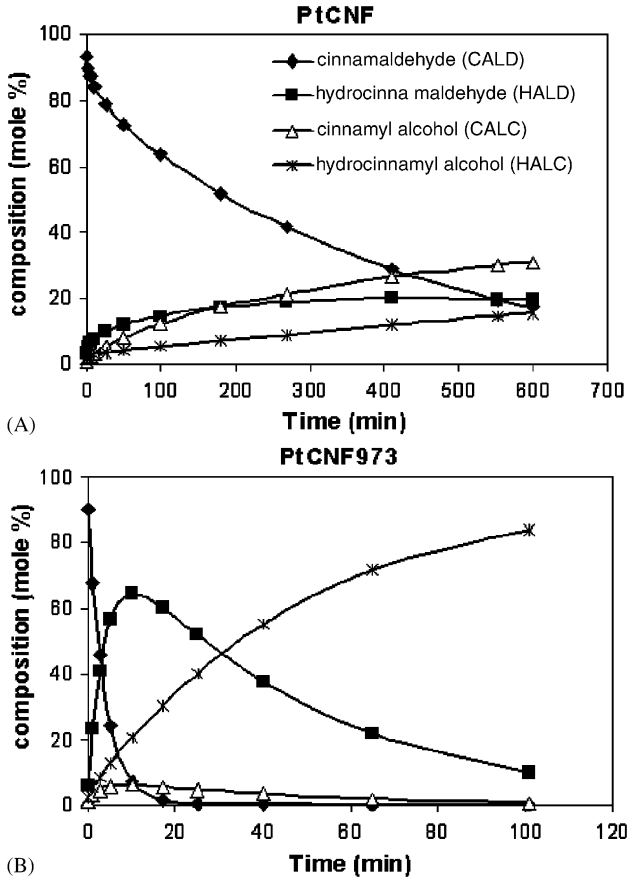

Fig. 2. Cinnamaldehyde conversion ($[CALD]_0 = 103$ mol/m^3) and product distribution as function of time on stream obtained at 383 K and a hydrogen pressure of 4.8 MPa over (A) PtCNF and (B) PtCNF973.

($[CALD]_0 = 345$ mol/m^3). From a comparison of the activities measured at 2.8 and 4.8 MPa for PtCNF it may be concluded that the rate is almost pressure independent, which might indicate that for this pressure range and catalyst hydrogen is not involved in the rate-determining step. However, the activity at a hydrogen pressure of 6.8 MPa is significantly higher, which point to a hydrogen order > 0. For PtCNF973 the influence of the hydrogen pressure is more pronounced, however, the order in hydrogen is < 1. The precise orders in hydrogen cannot be established from these data, for that more experiments would be required. The difference in hydrogen adsorption behavior is taken into account in our model by using for PtCNF and PtCNF973 orders in hydrogen of 0 and 0.5, respectively. With both catalysts no influence of the hydrogen pressure on the selectivities was observed.

3.2.3. Influence initial CALD concentration

In Fig. 4 the initial hydrogenation rates measured at 4.8 MPa and 383 K for both catalysts are plotted versus the initial CALD concentration ($[CALD]_0$). First, especially for PtCNF973, a strong increase in the initial activity with increasing $[CALD]_0$ is observed which levels off at higher

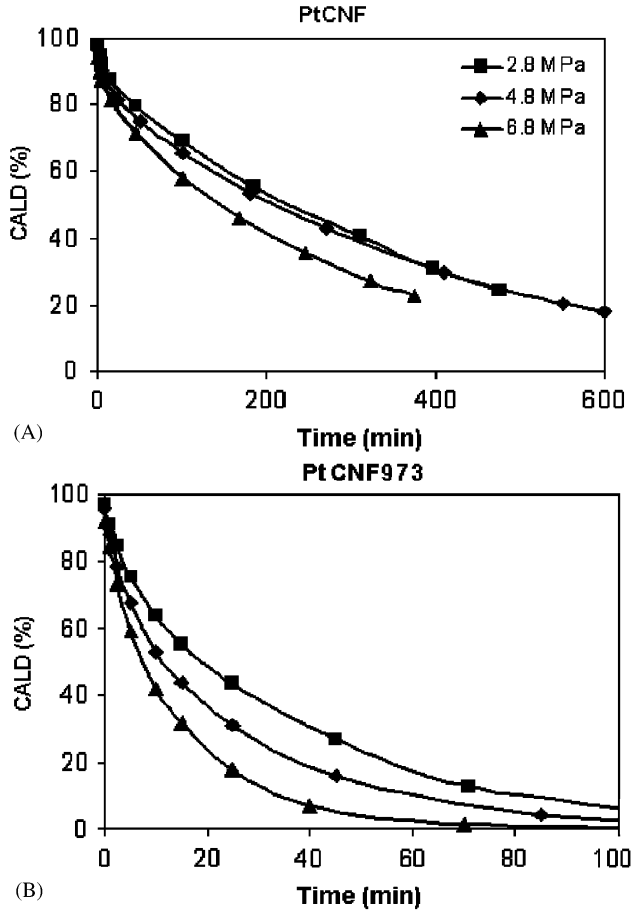

Fig. 3. Effect of hydrogen pressure on cinnamaldehyde conversion at 383 K over (A) PtCNF ($[CALD]_0 = 103\,mol/m^3$) and (B) PtCNF973 ($[CALD]_0 = 345\,mol/m^3$).

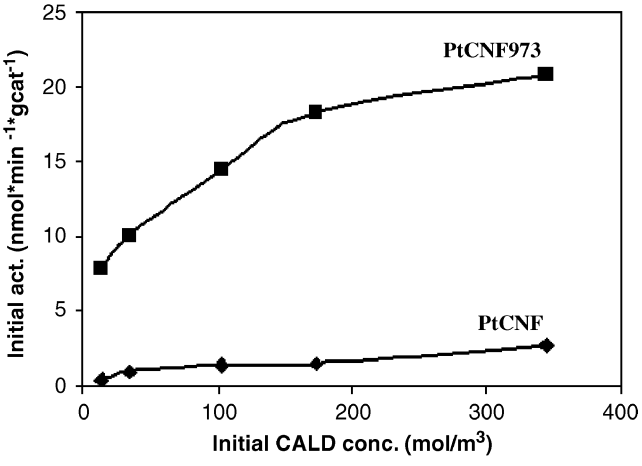

Fig. 4. Effect of initial CALD concentration on initial activity at 383 K and hydrogen pressure of 4.8 MPa for PtCNF and PtCNF973.

concentrations. This, again, is in accordance with LH adsorption kinetics, in which at low reactant concentrations the fractional occupancy of the catalyst surface increases linearly with the concentration in the solution and, with this, the activity. At higher reactant concentrations, however, the surface is almost fully occupied and the activity becomes independent of $[CALD]_0$.

The results collected in Fig. 5 show that not only the activity but also the selectivity is a function of the initial CALD concentration. For PtCNF S_{CALC} (Fig. 5A) increases with increasing CALD concentration at the expense of S_{HALD} (Fig. 5B) and S_{HALC} (not shown). With PtCNF973 S_{CALC} (Fig. 5C) is very small and practically independent of the initial CALD concentration. Nevertheless, S_{HALD} (Fig. 5D) changes drastically with $[CALD]_0$: the higher the initial CALD concentration, the higher S_{HALD}, although, beyond a CALD concentration of $173\,mol/m^3$ no further increase in S_{HALD} is observed. In literature a shift in selectivity for the CALD hydrogenation is ascribed to a change in adsorption mode with varying initial CALD concentration (Berger et al., 2001; Gallezot and Richard, 1998). At high concentrations the CALD molecules are supposed to adsorb perpendicular to the platinum surface with the aromatic rings in a parallel arrangement, thereby enhancing the hydrogenation rate of the carbonyl group. At low initial CALD the molecules are supposed to adsorb flat on the surface. For PtCNF an increase in S_{CALC} is observed with increasing $[CALD]_0$, which is in agreement with this model. However, in our study very small platinum particles are used, making the parallel arrangement of CALD molecules on the metal surface less probable. For PtCNF973, furthermore, S_{CALC} does not change and mainly S_{HALD} is increasing with the $[CALD]_0$. The shift in S_{HALD} is in the other direction, as one would expect from the model with the changing adsorption arrangement. An alternative explanation for the shift in selectivity with the concentration has been proposed by Nijhuis et al. (2003) who ascribed the dependency of the selectivities on the initial reactant concentration for the selective hydrogenation of 3-methyl-1-pentyl-3-ol to internal diffusion limitation of the organic reactant at the lowest concentrations. In case internal diffusion limitations of the organic reactant occur with PtCNF973 than an increased production of the final product HALC can be expected at the expense of CALC and HALD due to higher local concentrations of the intermediate products within the catalyst particles especially when using low $[CALD]_0$. This is in agreement with our results, making transfer problems very likely for PtCNF973.

3.2.4. Gas–liquid diffusion limitation

In the type of autoclave used, with a self inducing stirrer at 1500 rpm, a conservative estimate for the G–L mass transfer rate of hydrogen is $k_L a = 0.1\,s^{-1}$ (Ramachandran and Chaudhari, 1992). With a hydrogen concentration of $260\,mol\,m^{-3}$ ($P_{H_2} = 4.8$ Mpa; Young et al., 1981), a hydrogen transfer rate of about $26\,mol\,m^{-3}\,s^{-1}$ can be obtained. The highest measured rate is $0.31\,mol\,m^{-3}\,s^{-1}$. It can be calculated that in this case the bulk liquid would be 99%

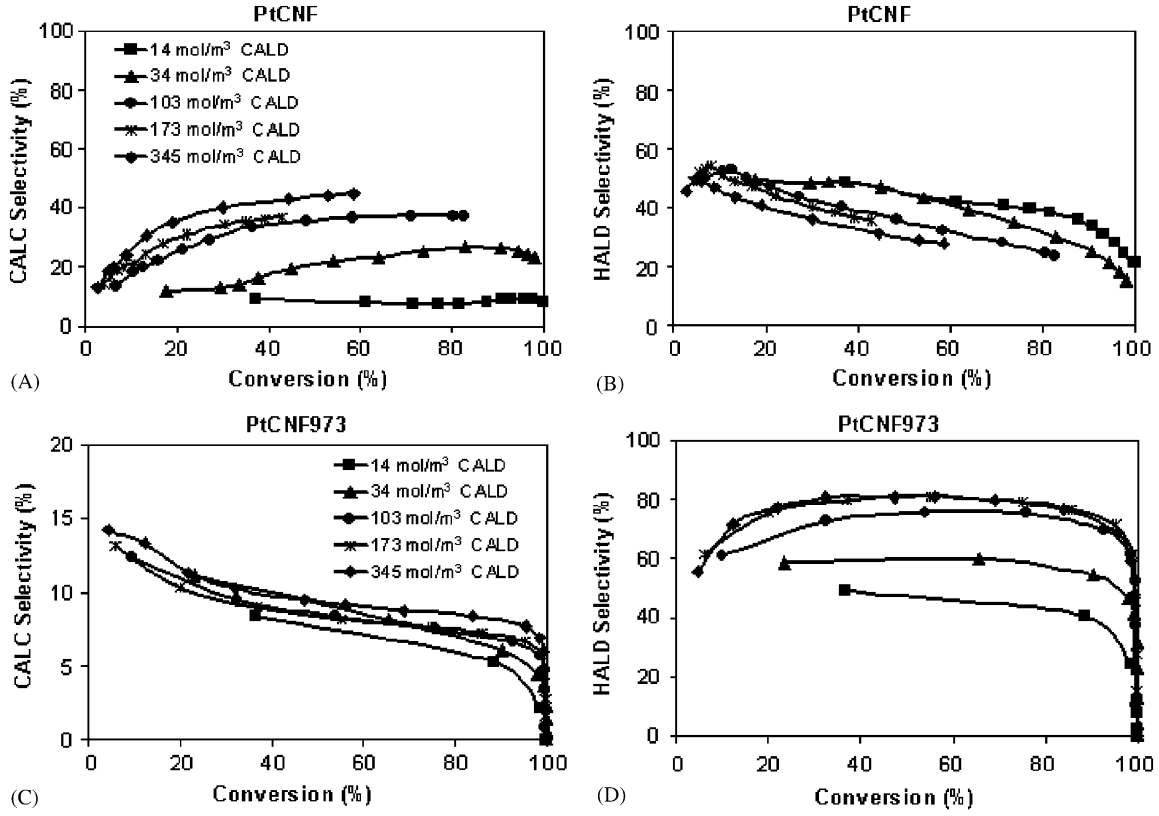

Fig. 5. Effect of initial CALD concentration on CALC and HALD selectivities for PtCNF (A) and (B) and PtCNF973 (C) and (D) ($T = 383\,\mathrm{K}$ and $P_{H_2} = 4.8\,\mathrm{MPa}$).

saturated with hydrogen, making G–L mass transfer limitation highly unlikely.

3.2.5. Intra-particle diffusion limitation

We stated as a possibility that the observed influence of the initial CALD concentration on the product selectivities could point towards internal diffusion limitations, especially with PtCNF973 since this catalyst is much more active than PtCNF. To evaluate the presence of internal diffusion limitations, we use the Weisz–Prater number

$$\Phi = \eta\phi^2 = \frac{\rho_p r_{v,\mathrm{obs}} d_p^2}{36 D_{\mathrm{eff}} c_s}\left(\frac{n+1}{2}\right) < 0.15. \quad (1)$$

In Table 1 the parameters used for the calculations are given. The diffusion coefficients for the organic compounds and hydrogen were estimated using the approximation method of Wilke and Chang (Wilke and Chang, 1955) and the effective diffusion coefficient (D_{eff}) was calculated according to $D_{\mathrm{eff}} = (\varepsilon_p/\tau)D$ (Table 1). In view of the Langmuir–Hinshelwood type of kinetics Weisz–Prater numbers were calculated for both an order of 0 and an order of 1.

The Weisz–Prater numbers (Φ) were calculated for hydrogen and CALD in the reaction performed under standard conditions ($T = 383\,\mathrm{K}$, $P_{H_2} = 4.8\,\mathrm{MPa}$). In these calculations the initial CALD concentration was used at which internal diffusion limitation is most probable ($[\mathrm{CALD}]_0 = 14\,\mathrm{mol/m^3}$). The results for both catalysts are given in Table 1. For PtCNF and PtCNF973 the Weisz–Prater numbers for hydrogen are smaller than 0.15, indicating the

Table 1
Weisz–Prater numbers (Φ) for hydrogen and CALD in the reaction performed under standard conditions ($T = 383\,\mathrm{K}$, $P_{H_2} = 4.8\,\mathrm{MPa}$ and $[\mathrm{CALD}]_0 = 14\,\mathrm{mol/m^3}$) with PtCNF and PtCNF973 and the parameters used for the calculations

Parameter	PtCNF	PtCNF973
ρ (kg/m^3)	1100	1100
$r_{w,\mathrm{obs}}$ (mol/(kg$_{\mathrm{cat}}$ s))	0.007	0.132
d_p (m)	120×10^{-6}	120×10^{-6}
ε_p	0.47	0.47
τ	2	2
$D_{\mathrm{eff,CALD}}$ (m^2/s)	2.0×10^{-9}	2.0×10^{-9}
D_{eff,H_2} (m^2/s)	8.4×10^{-9}	8.4×10^{-9}
c_{CALD} (mol/m^3)	14	14
c_{H_2} (mol/m^3)	260	260
n	0–1	0–1
S_{BET} (m^2/g)	186	186
Φ_{CALD}	0.05–0.11	1.1–2.1
Φ_{H_2}	0.0007–0.0013	0.013–0.027

absence of internal diffusion limitations. For CALD, on the other hand, using PtCNF a value close to 0.15 was found. Using PtCNF973 a value larger than 0.15 was obtained, pointing towards internal mass transport effects. These calculations are only an indication since the limit of 0.15 is not strict and the calculations are partly based on roughly estimated parameters. Therefore, intraparticle mass transfer is taken into account in the kinetic modeling.

3.3. Kinetic modeling

The kinetic experiments were modeled using the Athena Visual Workbench package (v. 8.0, Stewart & Associates Engineering Software). Based on the concentration–time results (Fig. 2) and the activity versus initial CALD concentration plot (Fig. 4) LHHW (Langmuir–Hinselwood–Hougen–Watson) kinetics were chosen, which is in agreement with literature (Tronconi et al., 1990; Neri et al., 1997; Vergunst et al., 2001). We assumed that hydrogen adsorption is dissociative and non-competitive with the organic molecules (i.e., on a separate site) and follows a Langmuir type of adsorption behavior. Amongst others Tronconi et al. (1990) and Neri et al. (1997) found that this gave the best results. For PtCNF973 an experimental order in hydrogen of approximately 0.5 is observed. This order of 0.5 implies that the rate-determining step (r.d.s.) involves a reaction with one adsorbed hydrogen atom that originates from dissociative adsorption of molecular hydrogen. For the PtCNF catalyst the experiments pointed towards an order in hydrogen close to 0, meaning that over this catalyst the reaction is almost independent of the hydrogen concentration. By using a large hydrogen adsorption constant (K_H) in the kinetic model an order in hydrogen of zero is simulated, while using a much smaller K_H will result in an order in hydrogen of 0.5. These values for K_H result in pseudo reaction orders of the model in agreement with the experimentally observed reaction orders.

Both a single- and a two-site model were investigated. In the single-site model C═C and C═O are hydrogenated on the same type of site and in the latter model two different types of sites for C═C and C═O hydrogenation are used. The best results were obtained with the single-site model, therefore we focused on this type of model for fitting our data. Other kinetic rate expressions (e.g. competitive hydrogen adsorption and a model for PtCNF973 without internal diffusion limitation) were also explored, but these expressions did not lead to satisfactory results.

Summarizing, the assumptions made to derive our kinetic model are:

- LH adsorption type kinetics.
- Only one type of site for the organic molecules is present. The hydrogenation of C═C and C═O occurs at the same site.

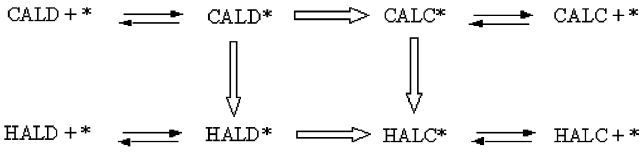

Fig. 6. The adsorbed species in the cinnamaldehyde hydrogenation model.

- The surface reactions are rate determining, adsorption and desorption are considered to be in quasi-equilibrium.
- Hydrogen shows dissociative adsorption that is not competitive with the organic reactants.
- Hydrogenation reactions using the primary products have shown that reactions are irreversible as is found in the literature (Vergunst et al., 2001; Gallezot and Richard, 1998).
- Spherical catalyst particles of uniform size.
- No G–L mass transfer limitations.
- R.d.s: reaction between an adsorbed organic species and one adsorbed hydrogen atom.

A scheme of the adsorbed species considered is depicted in Fig. 6. Since adsorption and desorption steps are in quasi-equilibrium a simplified reaction scheme can be utilized (Fig. 7).

According to the assumptions described above we have defined the reaction rate of the hydrogenation of CALD to HALD (reaction (1)) as

$$r_1 = k_1 \theta_{\mathrm{CALD}} \theta_H. \tag{8}$$

The number of active sites is included in the rate constant.

From Eq. (3) of the scheme (Fig. 7) it follows that

$$K_H = \frac{\theta_H^2}{\theta_\#^2 c_{H_2}} \rightarrow \theta_H = \theta_\# \sqrt{c_{H_2} K_H}$$

and with $\theta_\# + \theta_H = 1$ this results in

$$\theta_H = \frac{\sqrt{c_{H_2} K_H}}{1 + \sqrt{c_{H_2} K_H}}. \tag{9}$$

And from Eq. (4) we can derive

$$K_{\mathrm{CALD}} = \frac{\theta_{\mathrm{CALD}}}{\theta_* c_{\mathrm{CALD}}} \quad \theta_{\mathrm{CALD}} = c_{\mathrm{CALD}} K_{\mathrm{CALD}} \theta_* \tag{10}$$

Eqs. (5), (6) and (7) give, respectively,

$$\theta_{\mathrm{HALD}} = c_{\mathrm{HALD}} K_{\mathrm{HALD}} \theta_* \tag{11}$$

$$\theta_{\mathrm{CALC}} = c_{\mathrm{CALC}} K_{\mathrm{CALC}} \theta_* \tag{12}$$

$$\theta_{\mathrm{HALC}} = c_{\mathrm{HALC}} K_{\mathrm{HALC}} \theta_*. \tag{13}$$

The site balance is as follows:

$$\theta_* + \theta_{\mathrm{CALD}} + \theta_{\mathrm{HALD}} + \theta_{\mathrm{CALC}} + \theta_{\mathrm{HALC}} = 1. \tag{14}$$

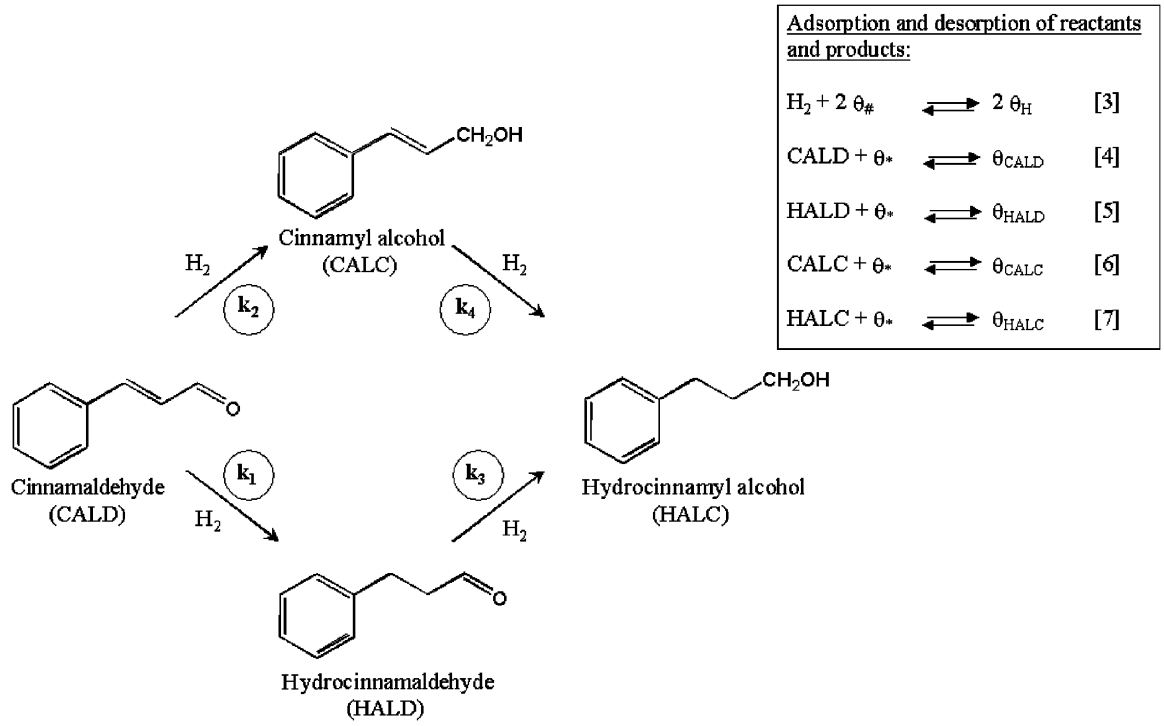

Fig. 7. Relevant reactions of the proposed kinetic model.

Combining (9)–(13) in the site balance equation results in

$$\theta_* = \frac{1}{1 + c_{\mathrm{CALD}}K_{\mathrm{CALD}} + c_{\mathrm{HALD}}K_{\mathrm{HALD}} + c_{\mathrm{CALC}}K_{\mathrm{CALC}} + c_{\mathrm{HALC}}K_{\mathrm{HALC}}}. \quad (15)$$

Using Eqs. (8)–(10) the rate expression for the hydrogenation of CALD to HALD (reaction (1)) can be derived

$$r_1 = k_1(c_{\mathrm{CALD}}K_{\mathrm{CALD}}\theta_*)\theta_H. \quad (16)$$

And with (9) and (15) this results in

$$r_1 = \frac{k_1 c_{\mathrm{CALD}}K_{\mathrm{CALD}}}{(1 + c_{\mathrm{CALD}}K_{\mathrm{CALD}} + c_{\mathrm{HALD}}K_{\mathrm{HALD}} + c_{\mathrm{CALC}}K_{\mathrm{CALC}} + c_{\mathrm{HALC}}K_{\mathrm{HALC}})} \frac{\sqrt{c_{H_2}K_H}}{1 + \sqrt{c_{H_2}K_H}}. \quad (17)$$

Analogously, the rate expressions of the hydrogenation of CALD to CALC (reaction (2)), HALD to HALC (reaction (3)) and CALC to HALC (reaction (4)) are

$$r_2 = \frac{k_2 c_{\mathrm{CALD}}K_{\mathrm{CALD}}}{(1 + c_{\mathrm{CALD}}K_{\mathrm{CALD}} + c_{\mathrm{HALD}}K_{\mathrm{HALD}} + c_{\mathrm{CALC}}K_{\mathrm{CALC}} + c_{\mathrm{HALC}}K_{\mathrm{HALC}})} \frac{\sqrt{c_{H_2}K_H}}{1 + \sqrt{c_{H_2}K_H}}, \quad (18)$$

$$r_3 = \frac{k_3 c_{\mathrm{HALD}}K_{\mathrm{HALD}}}{(1 + c_{\mathrm{CALD}}K_{\mathrm{CALD}} + c_{\mathrm{HALD}}K_{\mathrm{HALD}} + c_{\mathrm{CALC}}K_{\mathrm{CALC}} + c_{\mathrm{HALC}}K_{\mathrm{HALC}})} \frac{\sqrt{c_{H_2}K_H}}{1 + \sqrt{c_{H_2}K_H}}, \quad (19)$$

$$r_4 = \frac{k_4 c_{\mathrm{CALC}}K_{\mathrm{CALC}}}{(1 + c_{\mathrm{CALD}}K_{\mathrm{CALD}} + c_{\mathrm{HALD}}K_{\mathrm{HALD}} + c_{\mathrm{CALC}}K_{\mathrm{CALC}} + c_{\mathrm{HALC}}K_{\mathrm{HALC}})} \frac{\sqrt{c_{H_2}K_H}}{1 + \sqrt{c_{H_2}K_H}}. \quad (20)$$

The catalytic experiments have indicated that for PtCNF973 internal diffusion limitation is present; therefore we have included a term in our model for the diffusion of reactants and products in the catalyst particle. The differential equation for diffusion combined with reaction in a spherical catalyst particle is

$$\frac{\partial c}{\partial t} = D\left(\frac{\partial^2 c}{\partial z^2} + \frac{2}{z}\frac{\partial c}{\partial z}\right) - r_x. \quad (21)$$

Equations are solved in a spherical coordinate system (with radius z), for hydrogen and the organic reactant and products (each with their appropriate diffusivity). The reaction rate r_x, in which x is one of the organic compounds, is defined for CALD as $r_1 + r_2$, for HALD as $-r_1 + r_3$, for

CALC as $-r_2 + r_4$ and for HALC as $-r_3 - r_4$. The corresponding boundary conditions are:

$$z = 0 \rightarrow \frac{\partial c}{\partial z} = 0, \tag{22}$$

$$z = r_p \rightarrow c = c_s. \tag{23}$$

For hydrogen the bulk concentration is assumed to remain constant. The change in the bulk concentrations of the organic reactants/products is equal to the flux in/out of the catalyst particles. This can be described by the following differential equation for CALD:

$$\frac{\partial c_x}{\partial t} = -\frac{3}{r_p}\frac{c_{\text{cat}}}{\rho_{\text{cat}}} D_x \left.\frac{\partial c}{\partial z}\right|_{z=r_p} \tag{24}$$

with for all equations as starting values

$$t = 0, \quad c_{H_2} = c_{H_2,\text{sat}}, \quad c_x = c_{x,0}.$$

The differential equations were numerically solved and fitted to the experimental observations. The parameters that were fitted to the experiments are: k_1, k_2, k_3, k_4, K_{CALD}, K_{HALD}, K_{CALC}, K_{HALC}. Using PtCNF the K_H was assumed large (1.0×10^3) to represent the observed zero order in hydrogen and for PtCNF973 a small K_H (1.0×10^{-4}) was used to simulate the observed order in hydrogen of 0.5. In the experiments no inhibition of HALC was observed. To reduce the number of parameters, therefore the adsorption of the final product (HALC) was assumed to be zero. The diffusion coefficients for the organic compounds and for hydrogen used in the model amounted to $D_{\text{eff,CALD}} = 2 \times 10^{-9}\,\text{m}^2/\text{s}$ and $D_{\text{eff},H_2} = 8 \times 10^{-9}\,\text{m}^2/\text{s}$. A set of nine (PtCNF973), respectively, eleven (PtCNF) experiments were modeled simultaneously to determine the rate parameters and adsorption constants. The first two experimental points were not used for the fitting, since because of the high initial rate the relative uncertainty in the GC-analyses was considered too large as a result of small uncertainties in the sampling time. Consequently, the time axis was shifted by 3–5 min. Weighing factors were used in the fitting inversely proportional to $[\text{CALD}]_0$ so that all experiments were taken into account in the fitting process equally.

Some of the resulting fits (including the experimental data) for PtCNF are plotted in Fig. 8. From Fig. 8 it can be concluded that the model fits the experimental data fairly well. In Fig. 9 part of the fit results of PtCNF973 are plotted. In the experiment using 14 mol/m^3 CALD, the reactant is so rapidly converted that only the primary products (CALC and HALD) and the final product (HALC) are apparent in Fig. 9a. Also for this catalyst the fits are satisfactory.

The rate constants and adsorption constants of reactants and products are given in Table 2. The sum of the residual squares that is also shown in Table 2 gives information about the quality of the fit. Since the values are almost the same, the quality of the fits for PtCNF and PtCNF973 are comparable. From this table it is clear that changes of two to three orders of magnitude in reaction rate constants are obtained from the model for PtCNF and PtCNF973. For these parameters the 95% confidence intervals are given, demonstrating that these changes in the reaction rate constants are highly significant.

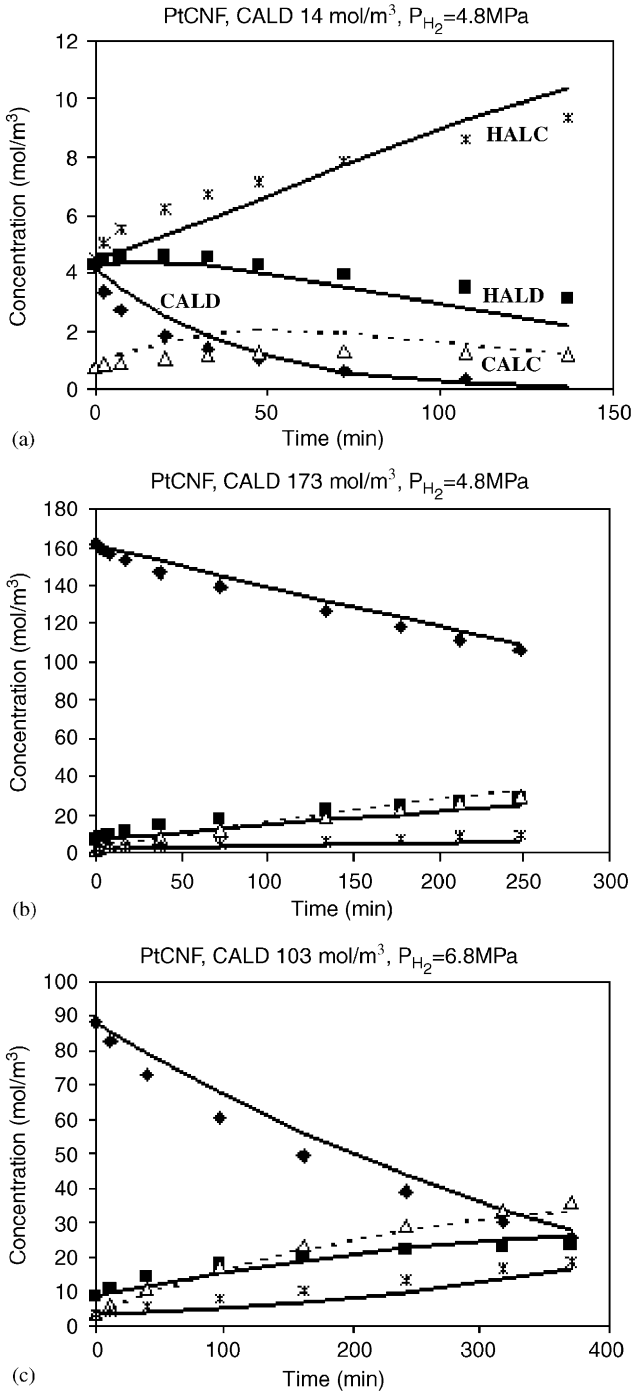

Fig. 8. Experimental and model results of some of the cinnamaldehyde hydrogenation reactions over PtCNF ($T = 383$ K). Line: Fitted according to the model, dotted line is CALC. Markers: Experimental data ♦ CALD, ■ HALD, △ CALC and ∗ HALC.

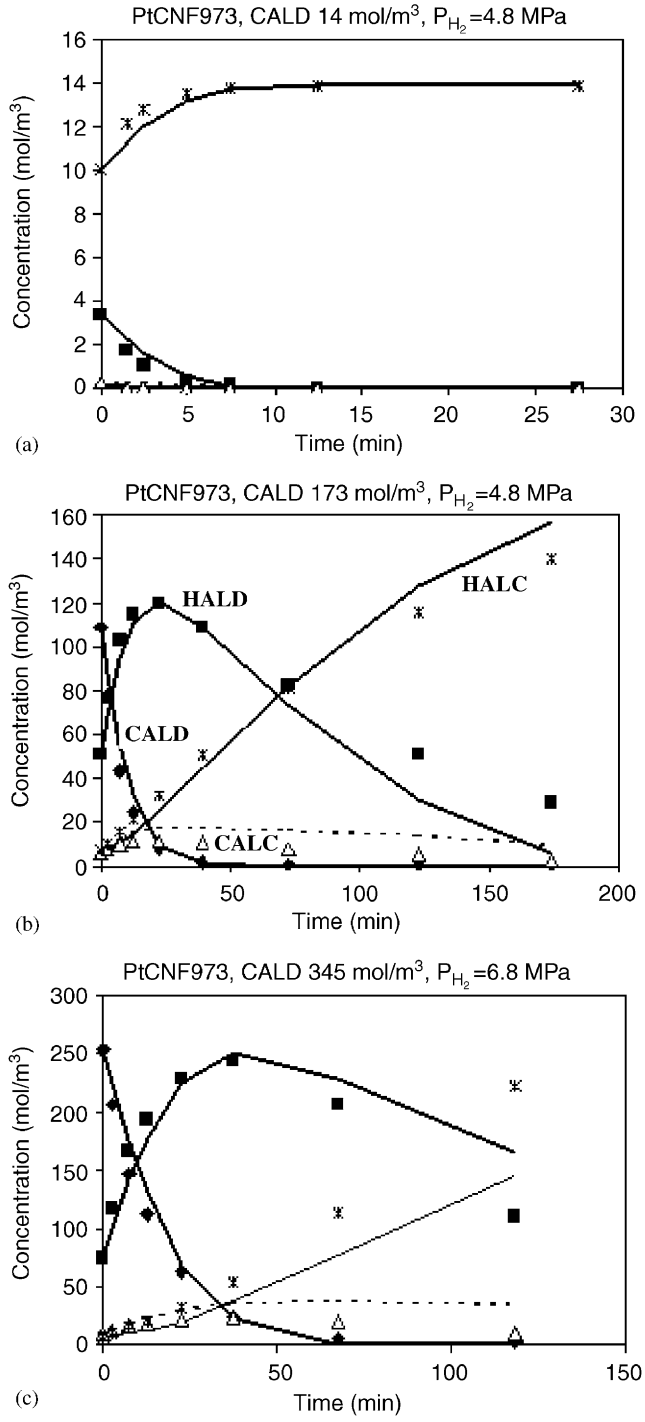

Fig. 9. Experimental and model results of some of the cinnamaldehyde hydrogenation reactions over PtCNF973 ($T = 383$ K). Line: Fitted according to the model, dotted line is CALC. Markers: Experimental data ♦ CALD, ■ HALD, △ CALC and ∗ HALC.

However, it is difficult to directly compare the reaction rate constants for the two catalysts, since they have a strong correlation with the adsorption constants, which are also changing. Therefore, a better comparison is made by calculating the intrinsic reaction rates from these parameters according to Eqs. (17)–(20). These intrinsic rates for selected process conditions are given in Table 3. When comparing the results obtained, especially the differences in r_1 and r_2 are striking. r_1 increases by a factor of about 120 with the removal of most of the oxygen groups from the CNF and r_2 increases by a factor of around 9. r_3 and r_4 also increase, it is to a lower extent.

The increases in intrinsic reaction rate can be caused by an increase in the catalyst activity, by an increase of the total number of active sites since this is included in the reaction rate constants, or by a combination of the two. Also a significant increase in the various adsorption constants is found going from PtCNF to PtCNF973. This indicates that after heat treatment the nature of the active sites has changed due to the removal of oxygen-containing groups. A working hypothesis based on the modeling results that can explain these differences in reaction rate and adsorption constants will be discussed in the last paragraph.

In Fig. 5A an increasing S_{CALC} with increasing conversion for PtCNF catalyzed reactions was observed. Our model cannot describe these results perfectly, since the kinetics used can only give rise to selectivities for CALC and HALD that decrease with increasing conversion. The observed behavior is an indication of either different sites for the carbonyl and olefinic bond hydrogenation, a change in the catalytic surface during the reaction, or changing modes of adsorption. It is, however, beyond the scope of this paper to investigate this behavior in detail, since the description of the model is sufficiently good to make an evaluation of the support effect.

3.3.1. Concentration profiles in the catalyst particle

Using the parameters of the model we report the calculated concentrations profiles inside the catalyst particles in the course of the various cinnamaldehyde hydrogenation experiments (Figs. 10a–d). In Figs. 10c and d the concentration profiles of H_2 of around 260 mol/m^3 have been omitted. For both PtCNF and PtCNF973 the hydrogen concentration throughout the particle remains practically constant. In PtCNF973 during reaction large concentration gradients of the organic compounds exist, especially when low $[CALD]_0$ are used, giving rise to internal transport limitations. The concentration profiles of PtCNF973 can also explain the shift in selectivities with $[CALD]_0$ as shown in Fig. 5D. If a low $[CALD]_0$ is used internal diffusion limitation results in accumulation of HALD in the catalyst particle. Because of the higher concentration this leads to large amounts of the secondary product HALC and a relatively low S_{HALD}. If, however, a larger $[CALD]_0$ is taken, internal transport limitation is less pronounced and HALD gradients are absent over the catalyst particle giving rise to a large S_{HALD}. In Fig. 10d the concentration profiles in a PtCNF particle are shown after 5 min reaction time when started with 14 mol/m^3 CALD. The concentration profiles here are much flatter than in Fig. 10c, demonstrating that with catalyst PtCNF internal

Table 2
The values of the estimated parameters in the kinetic models

Parameter	Units	PtCNF		PtCNF973	
			95% confidence interval		95% confidence interval
k_1	mol/(m^3_{cat} s)	2.0	1.7–2.3	1600	1400–1800
k_2	mol/(m^3_{cat} s)	3.3	3.0–3.6	210	150–280
k_3	mol/(m^3_{cat} s)	34	29–39	260	170–350
k_4	mol/(m^3_{cat} s)	1.5	1.1–1.9	16	1.6–30
K_{CALD}	m^3/mol	0.21		18	
K_{HALD}	m^3/mol	0.0078		5.7	
K_{CALC}	m^3/mol	0.21		18	
K_{HALC}	m^3/mol	0		0	
K_H	m^3/mol	1000		1.0×10^{-4}	
SSRES		8.9×10^4		1.0×10^5	

SSRES = Sum of squared residuals.

Table 3
Intrinsic reaction rates calculated from the modeled kinetic parameters ($c_{H_2} = 260\,mol/m^3$, $c_x = 103\,mol/m^3$, $T = 383\,K$)

Intrinsic reaction rate (mol/(m^3_{cat} s))	PtCNF	PtCNF973
r_1	1.9	220
r_2	3.2	29
r_3	15	36
r_4	1.4	2.2

diffusion limitation is hardly apparent. It should be noted that for batch-experiments these concentration profiles are dynamically changing in time, and that at the start of the experiments these concentration profiles as a result of mass transfer limitation are most steep. The reaction of 5 min shown in Fig. 10 is at an intermediate stage for the fastest reaction (50% conversion for PtCNF973), For PtCNF973 internal diffusion limitation implies that the observed activity is much lower than the intrinsic activity. This is confirmed by ratios up to 120 in the intrinsic reaction rates found using kinetic modeling, much larger than the factor 8 of the observed reaction rates of PtCNF973 versus PtCNF.

3.4. Support effects on catalytic performance

In part I of our study (Toebes et al., 2004a) on the influence of the oxygen-containing support surface groups on the performance of CNF-supported platinum catalysts in the hydrogenation of cinnamaldehyde we demonstrated that the amount of oxygen in the support does not influence the electronic state of the supported platinum to a large extent. Therefore, we concluded that the changes in catalytic properties are not primarily induced by an electronic effect (Toebes et al., 2004a). Our kinetic investigation reveals that with the removal of the oxygen from the graphite-like support the intrinsic reaction rates increase with a factor up to 120. It is difficult to discriminate whether this increase originates from an increase in the number of active sites or from an increase in intrinsic activity. This is because the reaction rate constants include the total number of active sites. H_2-chemisorption measurements and TEM demonstrate that the number of platinum sites is slightly smaller with PtCNF973, so it is impossible that an increase in the number of platinum active sites accounts for the strong increase in the reaction rate constants. However, if adsorption of the organic reactant with PtCNF973 can occur on the carbon support then the total number of adsorption sites may be enhanced. Nevertheless, it is unlikely that the total number of adsorption sites is increased by a factor of > 100. Therefore, we tentatively assign the increase in intrinsic reaction rates to both an increase in the total number of adsorption sites and an increase in the intrinsic activity.

Above observations and considerations are the basis for a model which can explain the enhanced activity for the high temperature treated catalyst. In Fig. 11 a schematic representation of our working hypothesis is depicted. It is assumed that on a CNF-supported platinum catalyst with a large amount of oxygen-containing surface groups (PtCNF) adsorption and dissociation of hydrogen and adsorption of the organic reactants all have to take place on the platinum particles. In other words the adsorption of CALD on the polar carbon surface is weak. On the platinum particles hydrogenation sites are present and apparently the hydrogenation of CALD on the platinum is rather difficult.

On the other hand, when hardly oxygen groups are present (PtCNF973), reactant molecules adsorb with the benzene ring on the non-polar surface of the carbon nanofibers. Hydrogen dissociation in all cases has to take place on the platinum particles. However, the organic reactants adsorbed in the vicinity of the platinum particles might easily and rapidly react with the hydrogen atoms adsorbed on the metal, resulting in an increased hydrogenation activity. So, hydrogenation is probably assisted by the CNF support due to adsorption of the substrate molecules on the surface. Theoretical calculations on the optimal geometrical configuration of CALD on the CNF surface, (Delbecq and Sautet, 2003), are needed to further study this proposition. Measurements

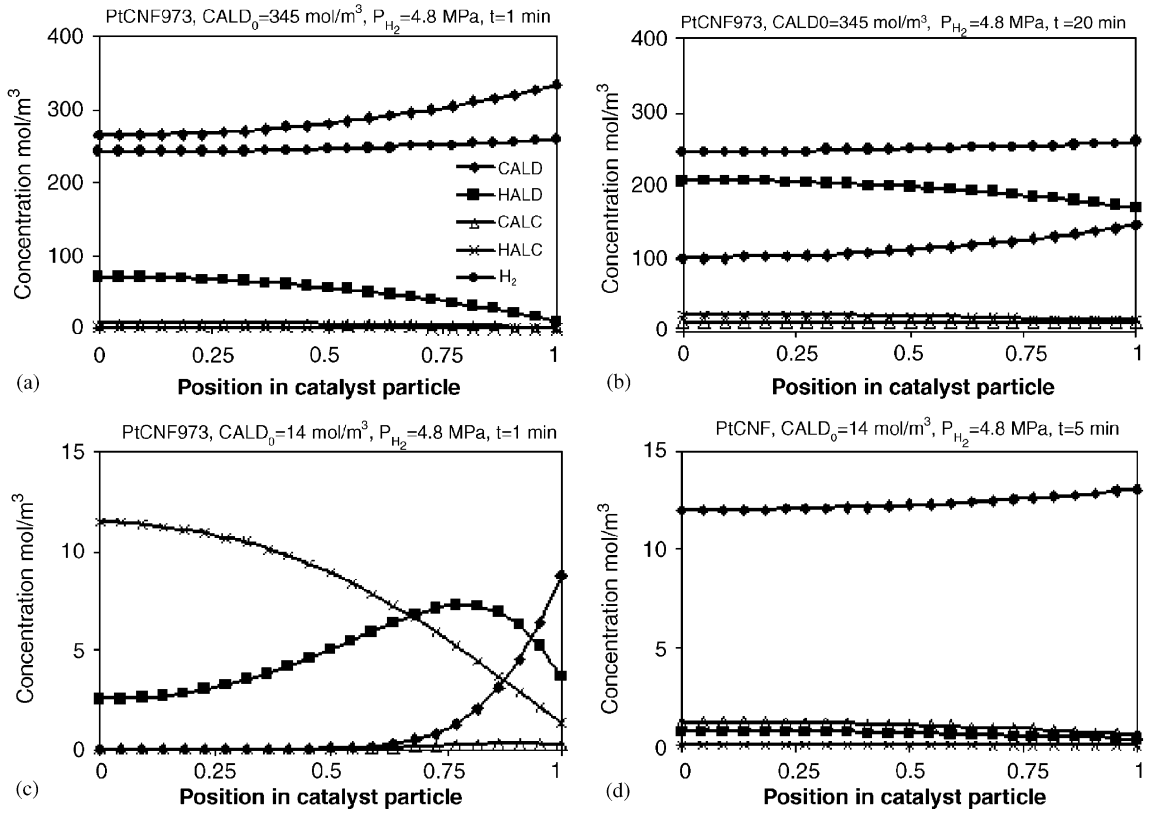

Fig. 10. Calculated concentration profiles in catalyst particles during cinnamaldehyde hydrogenation reaction performed at 383 K and a hydrogen pressure of 4.8 MPa (0 = center of catalyst particle; 1 = outside).

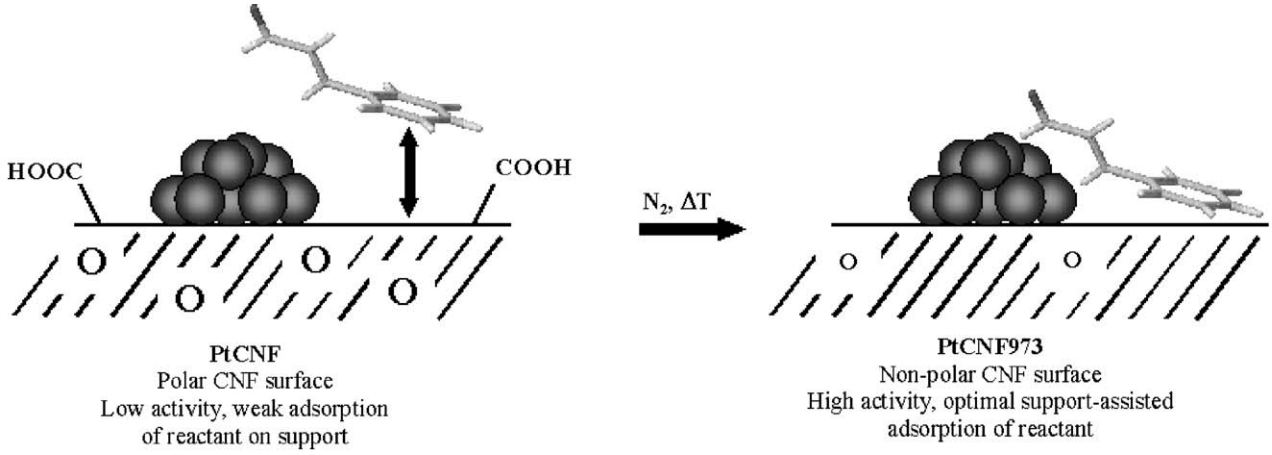

Fig. 11. Schematic representation of CALD adsorption explaining the enhanced activity for the CNF-supported platinum catalyst after the removal of the majority of the oxygen-containing groups, by support-assisted catalysis.

of the heat of adsorption of CALD on the two catalysts can contribute to this discussion too.

Finally, the experiments with various hydrogen pressures have displayed the difference in hydrogen dependency (PtCNF order in hydrogen of almost 0, PtCNF973 order in hydrogen of around 0.5) for the two catalysts, probably originating from a difference in the platinum-hydrogen adsorption strength. Although we could not find clear evidence for changes in electron properties of the platinum particles by partly removing the oxygen groups of the CNF support with XPS and H_2-chemisorption (Toebes et al., 2004a), it could not be fully ruled out that minor changes in the electronic properties are still important for catalysis by influencing the adsorption strength and mode of hydrogen on platinum.

4. Conclusions

Carbon nanofiber (CNF)-supported platinum catalysts with different concentrations of oxygen-containing surface groups on the support were employed to study the influence of these groups on the performance in the liquid-phase hydrogenation of cinnamaldehyde. The activity in this reaction was found to be strongly dependent on the amount of oxygen in/on the CNF support. The observed overall activity increased by a factor of 8 after removal of the majority of the oxygen groups by treatment at 973 K in inert atmosphere. The results showed a different hydrogen dependency for the two catalysts, demonstrating a change in the adsorption of hydrogen on platinum. Moreover, it was found that for PtCNF973 internal diffusion limitation of the organic compounds occurred, giving rise to an observed activity that is at least an order of a magnitude smaller than the intrinsic activity and gives rise to shifts in selectivity.

As results of our earlier study demonstrated that the amount of oxygen in the support does not influence the electronic state of the supported platinum to a large extent, we concluded that the changes in catalytic behavior are not primarily caused by an electronic effect. Using a single-site model based on Langmuir–Hinshelwood kinetics and taking into account mass transfer constraints with respect to the organic compounds we found that the intrinsic reaction rates increase up to a factor of 120 when the oxygen groups are removed from the CNF surface. Also the adsorption constants increased significantly, indicating that adsorption of cinnamaldehyde on PtCNF973 is stronger than on PtCNF. These results suggest that hydrogenation is assisted by adsorption of the benzene ring of cinnamaldehyde on the non-polar CNF support surface after removal of the oxygen-containing groups.

Notation

a	mass transfer area per reactor volume, $m^2/m^3_{reactor}$
c	concentration, mol/m^3
c_{cat}	catalyst concentration, $kg/m^3_{reactor}$
c_s	bulk concentration, $mol/m^3_{reactor}$
d_p	catalyst particle diameter, m
D	diffusion coefficient of diffusing compound in liquid, m^2/s
D_{eff}	effective diffusivity, m^2/s
k	reaction rate constant, $mol/(m^3\,s)$
k_L	mass transfer constant, m/s
K	adsorption equilibrium constant for compound on catalyst, m^3/mol
n	reaction order, dimensionless
r	reaction rate, $mol/(m^3_{cat}\,s)$
r_p	radius of the catalyst particle, m
$r_{w,obs}$	observed reaction rate, $mol/(s\,kg_{cat})$
S_{BET}	surface area determined by N_2-physisorption, m^2/g
t	time, s
z	radial position in catalyst particle, m

Greek letters

ε_p	porosity of particle
θ	fractional occupation, dimensionless
ρ_{cat}	catalyst density, kg/m^3_{cat}
ρ_p	catalyst particle density, kg/m^3
τ	porosity
Φ	Weisz–Prater number

Subscripts

$*$	empty site
cat	catalyst
CALD	cinnamaldehyde
CALC	cinnamyl alcohol
H_2	molecular hydrogen
HALC	hydrocinnamyl alcohol
HALD	hydrocinnamaldehyde
s	bulk
sat	saturation
x	organic compound

Acknowledgements

These investigations are supported by the Council for Chemical Sciences of the Netherlands Organization for Scientific Research with financial aid from the Netherlands Technology Foundation (CW/STW 349-5357).

References

Berger, R.J., Stitt, E.H., Marin, G.B., Kapteijn, F., Moulijn, J.A., 2001. Eurokin—Chemical reaction kinetics in practice. Cattech 5, 30–60.

Bitter, J.H., Seshan, K., Lercher, J.A., 1997. The state of zirconia supported platinum catalysts for CO_2/CH_4 reforming. Journal of Catalysis 171, 279–286.

Burch, R., Flambard, A.R., 1982a. Strong metal–support interactions in nickel/titania catalysts: the importance of interfacial phenomena. Journal of Catalysis 78, 389–405.

Burch, R., Flambard, A.R., 1982b. Some consequences of SMSI on the catalytic activity of nickel/titania catalysts. Studies in Surface Science and Catalysis 11, 193–201.

Cerveny, L., Belohlav, Z., Hamed, M.N.H., 1996. Catalytic hydrogenation of aromatic aldehydes and ketones over ruthenium catalysts. Research on Chemical Intermediates 22, 15–22.

Coq, B., Figueras, F., 1998. Structure-activity relationships in catalysis by metals: some aspects of particle size, bimetallic and supports effects. Coordination Chemistry Reviews 178–180, 1753–1783.

Coq, B., Kumbhar, P., Moreau, S., Moreau, P., Warawdekar, M.G., 1993. Liquid phase hydrogenation of cinnamaldehyde over supported ruthenium catalysts: influence of particle size, bimetallics and nature of support. Journal of Molecular Catalysis 85, 215–228.

Delbecq, F., Sautet, P., 2003. Influence of Sn additives on the selectivity of hydrogenation of α,β-unsaturated aldehydes with Pt catalysts: a density functional study of molecular adsorption. Journal of Catalysis 220, 115–126.

Gallezot, P., Richard, D., 1998. Selective hydrogenation of α,β-unsaturated aldehydes. Catalysis Reviews Science and Engineering 40, 81–126.

Galvagno, S., Capannelli, G., Neri, G., Donato, A., Pietropaolo, R., 1991. Hydrogenation of cinnamaldehyde over Ru/C catalysts: effect of Ru particle size. Journal of Molecular Catalysis 64, 237–246.

Giroir-Fendler, A., Richard, D., Gallezot, P., 1988. Selectivity in cinnamaldehyde hydrogenation of Group-VIII metals supported on graphite and carbon. Studies in Surface Science and Catalysis 41, 171–178.

Grunwaldt, J.-D., Baiker, A., 1999. Gold/titania interfaces and their role in carbon monoxide oxidation. Journal of Physical Chemistry B 103, 1002–1012.

Hajek, J., Kumar, N., Salmi, T., Murzin, D.M., Karhu, H., Vayrynen, J., Cerveny, L., Paseka, I., 2003. Impact of catalyst reduction mode on selective hydrogenation of cinnamaldehyde over Ru–Sn sol–gel catalysts. Industrial and Engineering Chemistry Research 42, 295–305.

Haruta, M., Tsubota, S., Kobayashi, T., Genet, M.J., Delmon, B., 1993. Low-temperature oxidation of CO over gold supported on TiO_2, α-Fe_2O_3, and Co_3O_4. Journal of Catalysis 144, 175–192.

Kluson, P., Cerveny, L., 1995. Selective hydrogenation over ruthenium catalysts. Applied Catalysis A-General 128, 13–31.

Koningsberger, D.C., Oudenhuijzen, M.K., de Graaf, J., van Bokhoven, J.A., Ramaker, D.E., 2003. In situ X-ray absorption spectroscopy as a unique tool for obtaining information on hydrogen binding sites and electronic structure of supported Pt catalysts: towards an understanding of the compensation relation in alkane hydrogenolysis. Journal of Catalysis 216, 178–191.

Kumbhar, P.S., Coq, B., Moreau, C., Moreau, P., Planeix, J.M., Warawdekar, M.G., 1995. Selectivity studies in hydrogenation of α,β-unsaturated aldehydes. In: Gupta, N.M., Chakrabarty, D.K. (Eds.), Catalysis: Modern Trends. Narosa Publishing House, New Delhi, pp. 541–547.

Marchi, A.J., Gordo, D.A., Trasarti, A.F., Apesteguia, C.R., 2003. Liquid phase hydrogenation of cinnamaldehyde on Cu-based catalysts. Applied Catalysis A-General 249, 53–67.

Mojet, B.L., Miller, J.T., Ramaker, D.E., Koningsberger, D.C., 1999. A new model describing the metal–support interaction in noble metal catalysts. Journal of Catalysis 186, 373–386.

Nijhuis, T.A., van Koten, G., Kapteijn, F., Moulijn, J.A., 2003. Separation of kinetics and mass-transport effects for a fast reaction: the selective hydrogenation of functionalized alkynes. Catalysis Today 79–80, 315–321.

Neri, G., Bonaccorsi, L., Mercadante, L., Galvagno, S., 1997. Kinetic analysis of cinnamaldehyde hydrogenation over alumina-supported ruthenium catalysts. Industrial and Engineering Chemistry Research 36, 3554–3562.

Poltarzewski, Z., Galvagno, S., Pietropaolo, R., Staiti, P., 1986. Hydrogenation of -α,β-unsaturated aldehydes over Pt–Sn/Nylon. Journal of Catalysis 102, 190–198.

Ponec, V., 1997. On the role of promoters in hydrogenations on metals; α,β-unsaturated aldehydes and ketones. Applied Catalysis A-General 149, 27–48.

Ramachandran, P.A., Chaudhari, R.V., 1992. Topics in Chemical Engineering, Vol. 2, Three-phase Catalytic Reactors. Gordon and Breach Science Publishers, Philadelphia.

Ramaker, D.E., de Graaf, J., van Veen, J.A.R., Koningsberger, D.C., 2001. Nature of the metal–support interaction in supported Pt catalysts: shift in Pt valence orbital energy and charge rearrangement. Journal of Catalysis 203, 7–17.

Toebes, M.L., Bitter, J.H., van Dillen, A.J., de Jong, K.P., 2002. Impact of the structure and reactivity of nickel particles on the catalytic growth of carbon nanofibers. Catalysis Today 76, 33–42.

Toebes, M.L., Prinsloo, F.F., Bitter, J.H., van Dillen, A.J., de Jong, K.P., 2003. Influence of oxygen-containing surface groups on the activity and selectivity of carbon nanofiber-supported ruthenium catalysts in the hydrogenation of cinnamaldehyde. Journal of Catalysis 214, 78–87.

Toebes, M.L., Zhang, Y., Hájek, J., Bitter, J.H., van Dillen, A.J., Murzin, D.Yu., Koningsberger, D.C., de Jong, K.P., 2004a. Support effects in the hydrogenation of cinnamaldehyde over carbon nanofiber-supported platinum catalysts: characterization and catalysis, part I. Journal of Catalysis 226, 215–225.

Toebes, M.L., van Heeswijk, M.N.H., Bitter, J.H., van Dillen, A.J., de Jong, K.P., 2004b. The influence of oxidation on the texture and the number of oxygen-containing surface groups of carbon nanofibers. Carbon 42, 307–315.

Tronconi, E., Crisafulli, C., Galvagno, S., Donato, A., Neri, G., Pietropaolo, R., 1990. Kinetics of liquid-phase hydrogenation of cinnamaldehyde over a Pt–Sn/nylon catalyst. Industrial Engineering and Chemistry Research 29, 1766–1770.

van de Moesdijk, C.M.G., Bosma, M.A.R., 1988. Process for the preparation of alpha–beta unsaturated alcohols, US Patent 4745234.

Van Dillen, A.J., Geus, J.W., Hermans, L.A.M., van der Meijden, J., 1977. Production of supported copper and nickel catalysts by deposition–precipitation. Proceedings of the Sixth International Congress on Catalysis 2, 677–685.

Vergunst, T., Kapteijn, F., Moulijn, J.A., 2001. Kinetics of cinnamaldehyde hydrogenation–concentration dependent selectivity. Catalysis Today 66, 381–387.

Wilke, C.R., Chang, P., 1955. Correlation of diffusion coefficients in dilute solutions. A.I.Ch.E. Journal 1, 264–270.

Young, C.L., Battino, R., Cargill, R.W., 1981. IUPAC Solubility Data Series, Vol. 5/6. Hydrogen and Deuterium. Pergamon, Oxford.

Zhang, L., Winterbottom, J.M., Boyes, A.P., Raymahasay, S., 1998. Studies on the hydrogenation of cinnamaldehyde over Pd/C catalysts. Journal of Chemical Technology and Biotechnology 72, 264–272.